Proceedings of the 7th International Symposium on Cavitation
CAV2009 – Paper No. 183
August 17-22, 2009, Ann Arbor, Michigan, USA

Incepting cavitation acoustic emissions due to vortex stretching

Natasha A. Chang
University of Michigan
Ann Arbor, MI, USA

Steven L. Ceccio
University of Michigan
Ann Arbor, MI, USA

ABSTRACT

The acoustic signal of cavitation bubbles can be characterized during inception, growth, and collapse. Growing and collapsing bubbles produced a sharp, broadband, popping sound. However, some elongated cavitation bubbles produced a short tone burst, or chirp, with frequencies on the order of 1 to 6 *kHz*. The frequency content of the acoustic signal during bubble inception and growth were related to the volumetric oscillations of the bubble and vortex dynamics coupling. A relationship was also found between the frequency of the oscillations and the flow and water quality conditions.

INTRODUCTION

The static pressure in the core of a linear vortex is depressed when compared with the pressure far from the vortex, and this pressure drop is increased if the vortex is stretched along its axis. In some cases, the pressure in the vortex core can fall below the liquid vapour pressure, resulting in a negative cavitation number. This can then lead to vortex cavitation if a small bubble or nucleus is present in this area of low pressure. Vortex cavitation bubbles may remain small compared with the vortex core radius, with the nearly spherical bubbles rapidly growing and collapsing within the vortex core. Or, when the bubble is exposed to a prolonged period of low pressure, the near spherical bubble can expand to fill the core of the vortex and then continue to grow along the vortex axis, becoming highly elongated. The growth, splitting, and collapse of vortex cavitation bubbles can produce a variety of acoustic emissions which can relate in complicated ways to the underlying vortical flow, the nature of the nucleus, and the possible presence of a time-varying pressure field in the far field (Chahine 1995; Choi & Chahine 2004; Choi, Hsiao, & Chahine 2004; Choi & Ceccio 2007; Choi, Hsiao, Chahine, & Ceccio 2009).

Concentrated regions of vorticity often occur in the tip regions of lifting surfaces immersed in liquid, and they are also associated with the flows within turbo-machinery and with turbulent jets, wakes, and shear layers. These are unsteady flows where vortex cavitation typically takes place before the onset of other forms of cavitation, such as, sheet cavitation or cloud cavitation. A review of this subject is provided by Arndt (2002). There are many instances in these unsteady flows where weaker or secondary vortices incept before the strongest vortices (*i.e.* the vortices with the highest circulation) in the flow. This is due to a variety of vortex-vortex interactions occurring between both co- and counter-rotating vortices of varying strength that can lead to stretching of smaller and weaker vortex filaments. These secondary vortices can produce cavitation at relatively high pressures due to both vortex stretching and axial flow acceleration in the vortex core. In the case of shear layers, the streamwise vortices can be an order of magnitude weaker than span wise vortices, but due to vortex interaction, the streamwise vortices will be stretched by the spanwise vortices and have been observed to cavitate well before the stronger spanwise vortices. The resulting cavitation inception location can occur at random sites throughout the shear layer (Katz & O'Hern 1986; O'Hern 1990; Golapan, Katz, & Knio 1999; Iyer & Ceccio 2002

Similarly, a recent study of a ducted rotor propulsor at the U. S. Navy's Naval Surface Warfare Center - Carderock Division (Chesnakas & Jessup 2003; Oweis, Fry, Chesnakas, Jessup & Ceccio 2006a and 2006b) show that the location and inception pressure of the cavitation was associated with the presence of multiple, interacting vortices. Moreover, Chesnakas & Jessup (2003) found that, depending on the static pressure surrounding the propulsor, the acoustic signal of the cavitation bubble was quite varied. As the static pressure was lowered from a condition of no cavitation, the initial bubble acoustic signatures resemble a "pop", a sharp broadband peak. As the pressure was further lowered the bubble signature took the form of a "chirp." An acoustic chirp was much longer in duration than a pop, and it contained a well-defined tone when compared to the broadband pop. The measured tone of a chirp was between 2 *kHz* to 6 *kHz* in frequency.

Vortex cavitation inception resulting in a well defined tone of frequencies lower than the resonant frequency of the bubble has been predicted analytically and numerically for cavitation bubbles in a line vortex by Choi *et al* (2009). In this study the interactions between a single cylindrical bubble in the core of a line vortex and the surrounding vortical flow were computed, including the redistribution of the vorticity surrounding the bubble due to the volume changes of the bubble. It was found that bubbles could undergo radial oscillation, during bubble growth and collapse. These radial oscillations would take place

with a period that was of the order of the vortex time scale $\tau_v = 2\pi r_c / u_{\theta,max}$, where r_c and $u_{\theta,max}$ are the (non cavitating) core radius and maximum tangential velocity. It was also found that the amplitude of this oscillation was related to the timescale of the pressure reduction that initiated the cavitation, ΔT, and the final core cavitation number, σ_c, once the minimum pressure was reached. As the core cavitation number decreases for a constant ratio of $\Delta T / \tau_v$, the amplitude of the radial oscillations increased. And for a constant core cavitation number, the amplitude of the oscillations increased as $\Delta T / \tau_v$ decreased.

EXPERIMENTAL SET UP

The experimental set up is described in detail in Chang et al. (2007) and Chang and Dowling (2009), therefore the following description is terse. The experiments were conducted in the University of Michigan 9-Inch Water Tunnel. The test section has a 22.9 *cm*, or approximately 9-inch, diameter inlet that smoothly transitions to a 22 by 22 *cm* rounded rectangular cross section. The length of the test section is 1 m. The test section has four acrylic windows that are 93.9 *cm* by 10.0 *cm* for viewing purposes. The flow speed and static pressure in the test section can be controlled to values between 0 to 18 *m/s* and from near vacuum to 200 *kPa*. A de-aeration system is used to control the dissolved oxygen content of the water.

The nuclei content of the free-stream flow was measured using a Cavitation Susceptibility Meter (CSM). The inferred size of the nuclei is that of a clean gas bubble which would cavitate at the same critical pressure. The water passing through the CSM was drawn at the height of the test section and upstream from the test, contraction, flow management, and first turning vanes sections. The CSM was located 1.8 m below the point where the water was drawn, and the water was returned to the lower leg of the channel.

The vortices were generated with two pairs, A and B, of non-standard but similar hydrofoils. Set A was conformed of two identical hydrofoils, and their rectangular plan-form was 95 *mm* in span and 167 *mm* in chord. Set B foils were 95 *mm* in span, and 167 and 134 *mm* in chord. The two hydrofoils were mounted on opposite side windows at the same height and location along the length of the test section. The trailing edges of the two foils end at the same distance along the test section length (Figure 1). The hydrofoil mounts allow rotation to achieve different angles of attack, creating counter-rotating vortex pairs with varying strengths. The span-wise gap between the two foils at zero angle of attack was 12.5 *mm*.

During the experiments, the water was de-aerated to achieve between 10% and 50% dissolved oxygen (DO) content at atmospheric pressure, which was measured with an Orion 810 dissolved oxygen meter. The free-stream flow velocity, U_∞, was set to 10 +/- 0.3 *m/s* yielding a chord-based Reynolds number of 1.67 x 10^6 based on the larger foil. The free-stream static pressure, P_∞, was varied to generate different cavitation numbers, and it ranged from 200 to 100 *kPa*. This corresponds to a free-stream cavitation number, σ_∞, ranging from 4 to 2, where P_V is the water vapour pressure and ρ is the water density:

$$\sigma_\infty = \frac{P_\infty - P_V}{\frac{1}{2}\rho U_\infty^2} \qquad (1)$$

Stereo Planar Particle Imaging Velocimetry (SPIV) was used to measure the vortical flow field in a plane downstream of the hydrofoils that was perpendicular to the flow direction. The location of the SPIV light sheet was 10 *cm* from the trailing edge of the foil, or approximately one chord-length (Figure 1).

Images of the vortex cavitation bubbles were acquired with two 8-bit Phantom V9.0 high-speed movie cameras with 50 *mm* or 85 *mm* focal length Nikon lenses in conjunction to 12 *mm* extension rings. The bubbles were illuminated from behind by four 300 W incandescent lights, and a light diffuser was used to prevent glare. The spatial resolution of the images varied depending on the effective resolution, frame rate, and the distance between the camera and the bubble being imaged. To generate a three-dimensional location of the bubbles imaged the cameras were focused in the same area of the tunnel but at right angles, from the side and from below, as shown in Figure 1. The movies were scaled by correlating the distance in pixels from the image of an immersed ruler at the approximate location of the bubbles. To study bubble dynamics, the cameras were set to acquire at 11000 fps images of 526 by 256 pixels for a 33 by 16 *mm* viewing area.

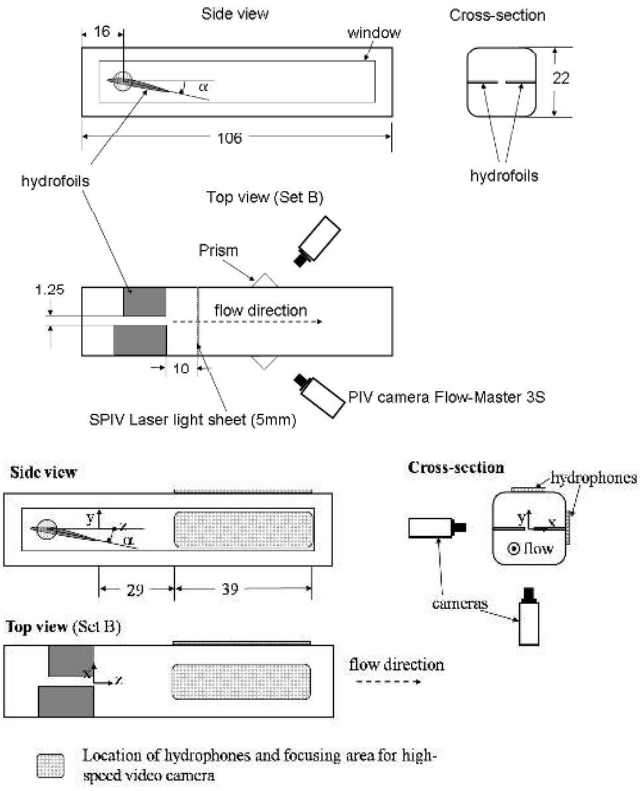

Figure 1: Hydrofoils and SPIV set up and acoustic array set up Dimensions are in *cm*.

An array of hydrophones was used to record the acoustic signal from the bubble. This array could determine the spatial position of sound-producing bubbles, to then compare with video data and ensure that the image corresponds to the sound recorded, Chang and Dowling (2009). The acoustic

localization array was comprised of 16 hydrophones, Reson TC-4013. The receiving sensitivity of the hydrophones is -211 +/- 3 *dB* re 1 *V μ/Pa* from 1 Hz to 170 *kHz*. To eliminate the 60 *Hz* noise signal from the power supply the preamplifier filter was set to 100 *Hz* high pass and 1 *MHz* low pass, and its gain set to 10 *dB*. The signal from the preamplifier is then filtered with a Khron-Hite 3364 four-pole tuneable active filter. The filter setting used was Butterworth high pass 1 *kHz*, and low pass 200 *kHz* with a 40 *dB* gain. Figure 1 shows the general locations of the hydrophones.

The acoustic and video data acquired is correlated in time. A common trigger, the acoustic signal of one of the receiving hydrophones, provided the synchronization of these two independent systems. The trigger event was a 1 *V* rising signal, which then prompted the video and acoustic systems to save their respective buffers. This data could then be used to compare the bubble dynamics with the sound it produces.

RESULTS AND DISCUSSION

The acoustic signal produced by the incipient cavitation was studied at dissolved oxygen contents less than 25% and high static pressure 157 *kPa* (σ_∞ = 3.1). The free stream flow speed was 10 *m/s*. The primary vortex circulation was -0.227 m^2/s, the secondary vortex circulation was 0.058 m^2/s. The core radius for the primary vortex is 6 *mm* and the secondary vortex is 3.7 *mm*. The distance between the vortices axes was 21 *mm*.

153 cavitation events were studied both acoustically in with high-speed video. The acoustic signal was strongest during inception and growth for 90% of the events, and during collapse for 10%. The acoustic signature that was detected at inception and growth exhibited both acoustic pops (42%) and the tonal bursts denoted as chirps in the introduction (48%). A pop corresponded to a sharp noise pulse of duration less than 2 *ms*, and a chirp corresponded to a periodic sound emission that lasted over 2 *ms*. The acoustic traces of the pops and chirps were qualitatively similar to those observed by Chesnakas and Jessup (2003) for the cavitation occurring in the tip region of a ducted rotor.

The signal-to noise ratio (SNR) was estimated for the 153 bubbles measured and categorized into the different events. The acoustic data was sampled by using a taper-to-constant duration Tukey window that was 300 points for a growth pop or collapse, or 2000 points for a chirp. The sample data was transformed with a 2^{12} point Fast Fourier Transform (FFT) with additional zero padding as required. The SNR was estimated with $\widetilde{M}(f) = \widetilde{S}(f) + \widetilde{N}(f)$ as the FFT of the sampled signal which inherently contains noise and noise samples $\widetilde{N}(f)$ windowed similarly. The SNR was then estimated with:

$$SNR(f) = 10\log_{10}\left(\frac{\left|\widetilde{M}(f)\right|^2 - \left|\widetilde{N}(f)\right|^2}{\left|\widetilde{N}(f)\right|^2}\right) \qquad (3)$$

Figure 2 shows the resulting data. It was found that the acoustic energy was concentrated at frequencies between 1 and 30 *kHz* at for a pop such as those recorded at inception, and between 2 to 6 *kHz* during bubble growth with a signal-to noise ratio (SNR) peak at approximately 3 *kHz*. The measured bubble collapses acoustic signal displayed a greater bandwidth than signals measured during growth. Though the growth pops and collapse show great overlap the maximum SNR value was measured at ~10 *kHz* and for a collapse was found to be ~2dB lower than the pop. From 100 Hz to 4 *kHz* the collapse SNR was higher than the pop. The acoustic emission of the cavitation bubbles was also related to the nuclei distribution. With higher dissolved oxygen content the nuclei are larger and more readily available. The resulting cavitation bubbles became more elongated, and their acoustic impulse during growth and collapse was weaker.

The strength of the acoustic signal is directly related to the volumetric acceleration of the bubble growth (Brennen, 1995):

$$P_A = \frac{\ddot{Q}\rho}{4\pi R} \qquad (4)$$

where, $\ddot{Q}$ is the volumetric acceleration of the bubble, and P_A is the estimated pressure at distance R from source. Ceccio & Brennen (1991) and Kuhn de Chizelle, Ceccio & Brennen (1995) discuss how the rapid collapse of traveling bubble cavitation lead to sharp acoustic pulses that are very similar to the pop type signal observed in the present study. And, Choi & Ceccio (2007) recorded similar acoustic traces for collapsing vortex cavitation bubbles. Oweis, Choi & Ceccio (2004) compared the sound produced by collapsing vortex cavitation bubbles to spherical bubbles with equivalent volume in an originally quiescent flow, and they found that when the bubbles remain nearly spherical in the core of the vortex, the noise producing efficiency of the bubbles approached that of the spherical bubbles. However, once the bubbles became significantly elongated, the intensity of the popping sound produced upon collapse was reduced.

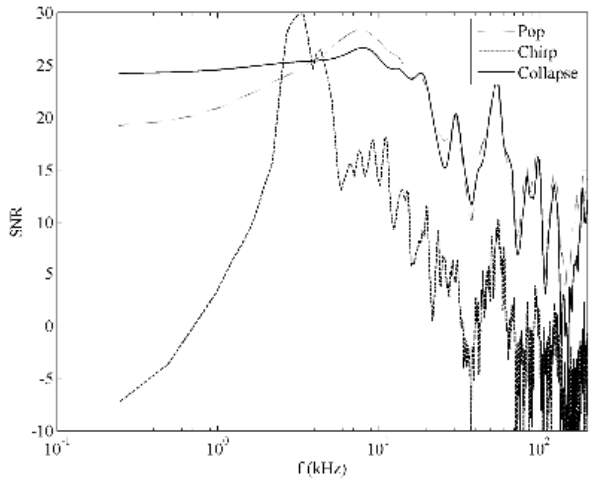

Figure 2: Signal-to-Noise Ratio of the distinct bubble dynamics and acoustic signature observed for the 153 counter-rotating vortex (CRV) bubbles measured at a dissolved oxygen of 25% and a σ_∞ = 3.1.

In Figure 3 the non-dimensional acoustic impulse of the 153 bubbles measured are plotted in conjunction with the data from Choi & Ceccio (2007), the acoustic impulse of the inception and collapse were found to be of the same magnitude and a order of magnitude larger than those measured in the

single line vortex experiment conducted by Choi & Ceccio (2007). In addition it was found in ~ 20% of the 153 bubbles with synchronized video and acoustic measurements that the strongest portion of their signature occurred when the bubble was arresting its growth and initiating collapse, and not at the initial growth or final collapse, see Figure 4.

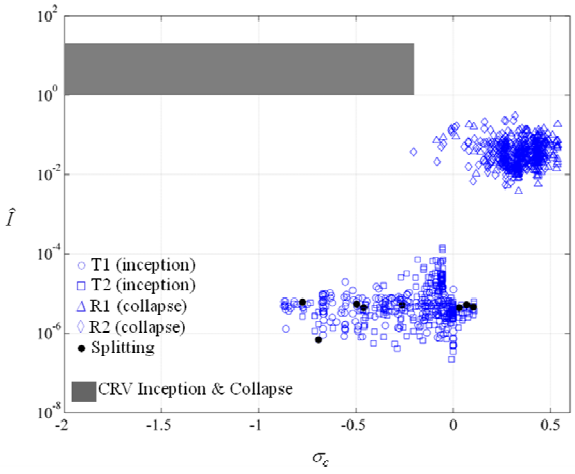

Figure 3: Figure reprinted from Choi & Ceccio (2007) showing in the grayed out area where the non-dimensional acoustic impulse, $\hat{I} = I_m r_H / (1/3\ \rho c \Delta P_c r_b^3 \theta)^{1/2}$, is estimated to be for the 153 counter-rotating vortex (CRV) bubbles cavitation inception and collapse measured at a dissolved oxygen of 25% and a $\sigma_\infty = 3.1$.

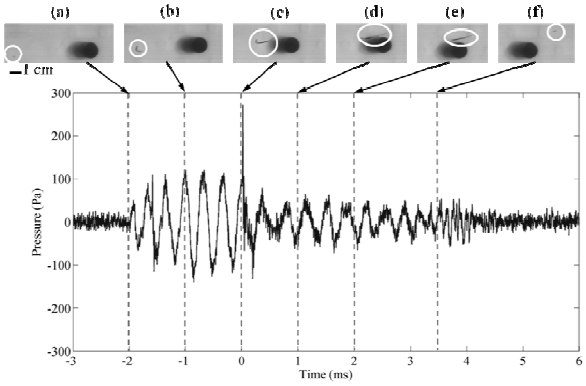

Figure 4: Time trace of a cavitation bubble acoustical signature. The give flow, a dissolved oxygen of 25% and a $\sigma_\infty = 3.1$. The (a) to (c) show the inception process where the bubble slowly grows and chirps. (c) The bubble experiences rapid growth and has a pop like signal, and then from (c) to (e) the bubble is slowly shrinking and producing a chirp like signature. Finally in (f) the bubble collapses, and its collapse was quieter than the initial growth or pop.

The single vortex cavitation bubbles studied by Choi & Ceccio (2007) did not exhibit any chirping type acoustic signal or loud inceptions. This difference can be ascribed to the variation in the nuclei populations and pressure histories in the vortex cores. The high tension required for initiating bubble growth in the secondary vortex leads to explosive nuclei growth. In turn, as the bubble grows it will redistribute the surrounding vorticity, causing the local core pressure to increase, retarding the bubble growth. If this process occurs slowly, the volumetric oscillations of the bubble may not produce a detectable sound pulse. Conversely, the explosive growth can lead to strong interactions with the surrounding vortical flow and cause bubble oscillations. The numerical and analytical study of bubble dynamics by Choi et al. (2009) examined the volume oscillations of two- and three-dimensional vortex cavitation bubbles, and they discuss how the radial volume oscillations of vortex cavitation bubbles occur with a timescale related to the underlying vortex properties:

$$\tau_V = \frac{2\pi r_C}{u_{\theta\max}} = \frac{4\pi r_C^2}{\beta\Gamma_0} \qquad (5)$$

where $\beta = 0.715$.

In the present experiment the 153 bubbles measured acoustically and with video, the oscillation frequency of the chirping bubbles is on the order of 2.5 to 5 *kHz*. Based on the measured flow properties, the change in the secondary vortex core radius that would account for the observed inception at pressures between 112 *kPa* and 157 *kPa* that correspond to $2.2 < \sigma_\infty < 3.1$ can be inferred. If the initial value of $r_{C,S} \sim 3.5$ *mm*, and with the assumption that the circulation is unchanged with a value of $\Gamma_S \sim 0.06$ m^2/s, the stretching would have to reduce the core radius to $0.6\ mm < r_C < 0.8\ mm$ to produce cavitation in the secondary vortex. Choi *et al.* (2009) showed how two-dimensional vortex cavitation had volume oscillations periods, T_p, between $0.6\tau_V < T_p < 1.4\tau_V$, while of a limited number of three-dimensional bubble simulations had periods on the order of $0.6\tau_V$. For the stretched secondary vortex the timescale would then be $1.1 \times 10^{-4}\ s < \tau_V < 1.8 \times 10^{-4}$ s, implying that the frequency of the chirp can range between $3.3\ kHz < 1/T_p < 12.7\ kHz$. The measured frequencies fall within the lower end of this range. Choi *et al.* (2009) showed that the oscillation frequency and amplitude depended on a number of flow parameters, including the original vortex circulation and core size, the core cavitation number, and the rate at which the core pressure was reduced. These parameters are not easily determined in the present study. Here, the measured volume oscillation period, T_p, was on the order of twice the inferred period of the stretched secondary vortex (*e.g.* ~2 τ_V) or half the inferred frequency. Hence, the measured sound frequency is lower, but on the same order, as that expected from the predicted secondary vortex properties. Finally, if the vortex stretching resulted in an axial flow in the core of the secondary vortex, the inferred core radius would be larger, and the inferred bubble oscillation frequency would be reduced. This is further circumstantial evidence that the reduction in the core pressure of the secondary vortex is due to a combination of a reduction in the core radius and the formation of axial jetting in the core.

The type of acoustic emission of the cavitation bubbles was observed to be related to the nuclei distribution and free-stream cavitation number for the given flow, see Figure 5. The ratio of bubbles that chirp to the total number of events was found to achieve a maximum value of ~0.5 for a dissolved oxygen content of 14% at σ_∞ of 2.5. At higher or lower σ_∞ the ratio was lower. To achieve the ~0.5 ratio of chirping bubbles to total number of cavitation events at 44% dissolved oxygen content the σ_∞ was 3.6 It was not possible to test higher σ_∞ to see if the ratio would correspondingly drop. In addition, it was observed for the 44% dissolved oxygen case that as the ratio increased to its ~0.5 maximum, the period of the chirp changed in relation to the σ_∞. At the lower σ_∞ the periods of chirps tended to be longer, some up to 1 *ms* long ($\sigma_\infty = 2.2$), and as the σ_∞ was increased the average period of the chirp would decrease, to a minimum observed value of 0.1 ms ($\sigma_\infty = 3.6$).

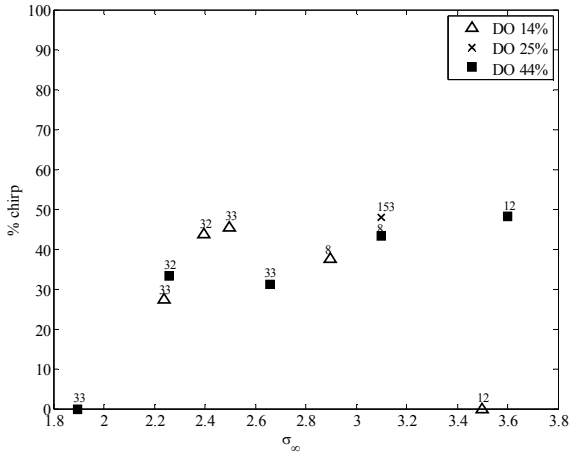

Figure 5: % of chirps observed at different free-stream cavitation numbers and dissolved oxygen content (DO). The data was acquired at 500 *MHz* at 3 *s* intervals. More data was required for higher cavitation numbers or lower DO. The acoustic events were detected if the signal was 20 *dB* higher than the noise. The number on top of the symbol corresponds to the number of cavitation events detected.

CONCLUSION

The acoustic emissions of an incepting cavitating vortex were measured and compared to video data. It was found that low frequency tones can take place during the inception and growth of a cavitating bubble. These finding were related to a coupling between the bubble dynamics and the vortex dynamics that was numerically observed in Choi *et al* (2009).

In addition, it is shown that the cavitating bubble's likelihood of emitting a chirp varied with the water conditions and free-field cavitation number, and that the frequency of its chirp also varied following the trends postulated by equation (5). The present results, when combined with those of previous studies, illustrate a potential limitation of conventional vortex-cavitation scaling based solely on "water quality" and the Reynolds number. The simplest scaling for water quality is based on the ratio of the length scales between the model and the prototype flows, λ. Here, the nuclei density of the prototype scale should be λ^3 that of the model scale. Implicit in this scaling is the notion that all nuclei will cavitate in a similar fashion and produce the same bubble dynamics and acoustic emissions, especially when the nuclei populations are such that they produce "weak water". However, if the water on the prototype scale is not rich in large nuclei, the resulting vortex cavitation may be quite different than that on the model scale, even if the nuclei densities are scaled properly. This is illustrated by the significant variety of the dynamics and emissions of the bubbles observed in the present study and of those observed by Choi & Ceccio (2007).

ACKNOWLEDGMENTS

The Office of Naval Research supported this work under grant number N00014-03-1-0430, Dr. Ki-Han Kim, Program Manager. The authors would also like to acknowledge Dr. Jaehyug Choi and Dr. Ryo Yakushiji for their assistance.

REFERENCES

Arndt, R.E.A. 2002 Cavitation in vortical flow, *Annu. Rev. Fluid Mech.* **34**, pp 143–175.

Brennen, C.E. 1995 Cavitation and bubble dynamic. Oxford University Press, New York,

Ceccio, S. L. & Brennen, C. E. 1991 Observations of the dynamics and acoustics of travelling bubble cavitation. *J. Fluid Mech.* **233**, 633–660.

Chahine, G. L. 1995, Bubble interactions with vortices, *Vortex Flows*, S. Green, Editor, Klewer Academic, **30**, 783-823

Chang, N.A. & Dowling, D.R. 2009 Ray-based acoustic localization of cavitation in a highly reverberant environment *J. Acoust. Soc. Am.* **125**, pp.3088-3100

Chang, N.A., Choi, J., Yakushiji, R., Dowling, D.R. and Ceccio, S.L., 2007 Dynamics and noise emission of cavitation bubbles in multiple vortex flow, *6th International Conference on Multiphase Flow*, I*CM*F, Leipzig, Germany, July 9 – 13, 2007

Chesnakas, C., & Jessup, S. 2003 Tip vortex induced cavitation on a ducted propulsor. *Proc. 4th ASME-JSME Joint Fluids Eng. Conf.*, FEDSM2003-45320, Honolulu, Hawaii, 2003

Choi, J. K. & Chahine, G. L. 2004, Noise due to extreme bubble deformation near inception of tip vortex cavitation. *Physics of Fluids*, **16** (7), 2411-2418

Choi, J. K., Hsiao, C.-T. & Chahine, G. L. 2004 Tip vortex cavitation inception study using the Surface Averaged Pressure (SAP) model combined with a bubble splitting model. *Proc. 25th Symposium on Naval Hydrodynamics*, CANADA

Choi, J. and Ceccio, S.L., 2007 Dynamics and noise emission of vortex cavitation bubbles, *Journal of Fluid Mechanics*, Vol. **575**, pp 1-26

Choi, J., Hsiao, C.-T., Chahine, G., & Ceccio, S. L. 2009 Growth, oscillation, and collapse of vortex cavitation bubbles. *J Fluid Mech.* **624**, 255-279

Gopalan, S., Katz, J. &. Knio, O 1999 The flow structure in the near field of jets and its effect on cavitation inception, *J. Fluid Mech.* **398**, 1-43

Iyer, C.O. and Ceccio, S.L. 2002 The Influence of Developed Cavitation on the Flow of a Turbulent Shear Layer, *Phys. of Fluids*, Vol. **14** (10), pp 3414–3431

Katz, J. & O'Hern, T. J. 1986 Cavitation in large scale shear flow. *Trans. ASME J. Fluids Eng.* **108** (3), 373-376

Kuhn de Chizelle, Y., Ceccio, S. L. & Brennen, C. E. 1995 Observations and scaling of travelling bubble cavitation. *J. Fluid Mech.* **293**, 99–126.

O'Hern, T. J. 1990 An experimental investigation of turbulent shear flow cavitation. *J. of Fluid Mech.* **215**, 365-391

Oweis, G.F., Choi, J. & Ceccio, S.L. 2004 Dynamics and noise emission of laser induced cavitation bubbles in a vortical flow field. *J. Acoust. Soc. Am.* **115** (3), 1049-1058

Oweis, G.F., Fry, D., Chesnakas, C.J., Jessup, S.D. & Ceccio, S.L. 2006a Development of a Tip-Leakage Flow—Part 1: The Flow Over a Range of Reynolds Numbers. *J. Fluids Eng*. **128**, 751-765

Oweis, G.F., Fry, D., Chesnakas, C.J., Jessup, S.D. & Ceccio, S.L. 2006b Development of a Tip-Leakage Flow: Part 2-Comparison between the Ducted and Un-ducted Rotor. *J. Fluids Eng.* **128**, 765-773